Determination of the time-dependent reaction coefficient and the heat flux in a nonlinear inverse heat conduction problem

L. Zhuo[a,b]; D. Lesnic[b] ; M. I. Ismailov[c]; I. Tekin[d] and S. Meng[a]

[a]Center for Composite Materials and Structures, Harbin Institute of Technology, Harbin 150080, China; [b]Department of Applied Mathematics, University of Leeds, Leeds LS2 9JT, UK; [c]Department of Mathematics, Gebze Technical University, Gebze-Kocaeli 41400, Turkey; [d]Department of Mathematics, Bursa Technical University, Yildirim-Bursa 16310, Turkey

ABSTRACT

Diffusion processes with reaction generated by a nonlinear source are commonly encountered in practical applications related to ignition, pyrolysis and polymerization. In such processes, determining the intensity of reaction in time is of crucial importance for control and monitoring purposes. Therefore, this paper is devoted to such an identification problem of determining the time-dependent coefficient of a nonlinear heat source together with the unknown heat flux at an inaccessible boundary of a one-dimensional slab from temperature measurements at two sensor locations in the context of nonlinear transient heat conduction. Local existence and uniqueness results for the inverse coefficient problem are proved when the first three derivatives of the nonlinear source term are Lipschitz continuous functions. Furthermore, the conjugate gradient method (CGM) for separately reconstructing the reaction coefficient and the heat flux is developed. The ill-posedness is overcome by using the discrepancy principle to stop the iteration procedure of CGM when the input data is contaminated with noise. Numerical results show that the inverse solutions are accurate and stable.

CONTACT D. Lesnic. Email: amt5ld@maths.leeds.ac.uk

Nomenclature

d^n	direction of descent at nth iteration
E_1, E_2	accuracy errors
$f(x,t)$	heat source
f_i^j	heat source at $\tilde{x}_i$ and t_j
$g(u)$	temperature-dependent reaction function
$h(t)$	reaction coefficient
h^j	reaction coefficient at t_j
J_1, J_2	objective function
J_i'	gradient of J_i
M	number of nodes in space domain
N	number of nodes in time domain
n_h, n_q	stopping iteration numbers
$n_{\mathrm{opt},h}$	optimal iteration number for $h(t)$
$n_{\mathrm{opt},q}$	optimal iteration number for $q(t)$
P	function needed to be estimated
p	percentage of noise
$q(t)$	heat flux
q^j	heat flux at t_j
r	ratio of Δt to $(\Delta x)^2$
t	time variable
t_j	jth temporal node
T	final time of interest
$u(x,t)$	temperature
u_i^j	temperature at $\tilde{x}_i$ and t_j
u_0	initial temperature
x	space variable
x_1, x_2	coordinates of measurement points
$\tilde{x}_i$	coordinate of ith spatial node
Y_1, Y_2	measured temperatures

Greek symbols

β^n	search step size at nth iteration
χ	power order
δ	Dirac delta function
Δx	mesh size in space domain
Δt	mesh size in time domain
$\mathcal{E}_i$	tolerance of J_i
ϵ_i	measurement noise of Y_i
ε	small parameter
γ^n	conjugate coefficient at nth iteration
Λ	eigenvalue
$\lambda(x,t)$	Lagrange multiplier
σ_i	standard deviation of noise ϵ_i

1. Introduction

Inverse heat conduction problems (IHCP) associated with the estimation of boundary functions (e.g. temperature, heat flux, surface heat transfer coefficient) [3, 5] arise in various areas of applied thermal engineering. One of the typical applications concerns the reconstruction of exterior thermal environment of heat shields on re-entry vehicles using internal temperature measurements. Furthermore, the heat transfer process can also be influenced by a heat source, which may or may not depend on the temperature, whose identification is referred to as the inverse heat source problem (IHSP). Typical applications of IHSPs occur in bio-heat conduction [36, 42], fins in heat exchangers [27, 28], microwave heating [45], mass transport in groundwater [39], spontaneous ignition [31], pyrolysis of ablative materials [33] and polymerization of bone cements [22].

The unknown boundary conditions and the source term are desired to be determined from temperature measurements on the surface or inside the spatial domain. The analysis of inverse problem requires the solution of its corresponding direct problem, which is concerned with the determination of the effect (temperature) from known cause (boundary condition and source term). Although some analytical methods are available for solving the heat conduction equation to establish the relationship between internal temperature and boundary heat flux [15, 16, 24, 48], the analytical solution can hardly be obtained when there exists a nonlinear heat source (temperature-dependent). Fortunately, a number of numerical methods have been employed to deal with such kind of problems [29, 31, 38, 46]. Because of the ill-posed nature of inverse problem, small errors in the experimental measurements cause large oscillations in the inverse solution. Therefore, many methods have been proposed to address the instability of the solution, e.g., Tikhonov's regularization [40], function specification method [3], truncated singular value decomposition (TSVD) [18], Levenberg-Marquardt algorithm (LM) and conjugate gradient method (CGM) [30].

When the heat source does not depend explicitly on the temperature, the resulting linear IHSPs of identifying space-dependent and time-dependent coefficient have been rigorously investigated in [14] and [21], respectively. Especially, in [21], the well-posedness of the inverse problem was established based on some assumptions over the input data. Moreover, Hasanov [20] considered the identification of the space and time dependent sources in two seperate inverse problems, which were numerically solved based on CGM and collocation algorithm, respectively. On the other hand, when the heat source depends linearly on the temperature, the source term with an unknown time-dependent control function was solved using various finite difference schemes [12, 44]. As an example, Trucu et al. [42] identified the space-dependent blood perfusion coefficient using the Crank-Nicolson finite difference scheme combined with the Tikhonov regularization method. More recently, Cao and Lesnic [7] reconstructed the space and time-dependent blood perfusion coefficient using the CGM.

When the heat source depends nonlinearly on the temperature the literature on IHSP for the resulting semilinear heat equation is rather scarce [8, 22, 35, 37]. For the numerical solution, Huang et al. [22] applied the CGM to determine the heat source governed by the Arrhenius law, but the source term was assumed an explicit function of space and time variables. Shidfar et al. [37] used the LM algorithm to approximate the space-dependent nonlinear source in a special basis functions space. Our work will show rigorously the local existence and uniqueness of the time-dependent intensity of a nonlinear reaction process from internal temperature measurements, which has not been investigated yet to our knowledge. Besides, it should be noted

that all the aforementioned works concerned with source identification are based on the assumption of known boundary conditions. But in some circumstances, the boundary conditions are also unknown as the measurement on the surface is inaccessible [47].

To summarise, the aim of this article is to investigate the inverse problem of determining the time-dependent coefficient of a nonlinear source and the heat flux in a nonlinear parabolic equation from two temperature measurements in time. The numerical method for solving the direct problem of heat conduction with nonlinear source based on the FDM is presented in section 2. In section 3 the inverse problems under investigation are formulated. The local existence and uniqueness of a classical solution to the IHSP are proved in section 4 and the numerical CGM for solving the inverse problems is presented in section 5. Two numerical examples are illustrated to verify the accuracy and stability of the algorithm in section 6. Finally, conclusions are presented in section 7.

2. Direct problem

Consider the one-dimensional direct heat conduction problem in a homogeneous finite slab of unit length with a nonlinear source given by:

$$\frac{\partial u}{\partial t} = \frac{\partial^2 u}{\partial x^2} + h(t)g(u) + f(x,t), \quad (x,t) \in [0,1] \times [0,T], \tag{1}$$

subject to Neumann heat flux boundary conditions

$$-\frac{\partial u}{\partial x}(0,t) = q(t), \quad t \in (0,T], \tag{2}$$

$$\frac{\partial u}{\partial x}(1,t) = 0, \quad t \in (0,T], \tag{3}$$

and initial condition

$$u(x,0) = u_0(x), \quad x \in [0,1], \tag{4}$$

where $T > 0$ is a final time of interest, $f(x,t)$ is a free term heat source, $u(x,t)$ is the dependent variable, i.e., the temperature, $g(u)$ is an a priori known heat source/reaction function depending on u given by some physical/chemical laws, and $h(t)$ is a time-dependent reaction coefficient characterizing the intensity of the source term. The initial temperature is $u_0(x)$. The boundary at $x = 0$ is subjected to a time varying heat flux $q(t)$, whilst the boundary at $x = 1$ is insulated.

Because of the presence of the nonlinearity $g(u)$, no analytical method is available and hence the finite difference method (FDM) is applied for numerical discretization. The mesh sizes in space and time domains are $\Delta x = 1/(M-1)$ and $\Delta t = T/(N-1)$, where M and N denote the number of nodes. The nodes are $\tilde{x}_i = (i-1)\Delta x$, $i = 1 \text{ to } M$ and $t_j = (j-1)\Delta t$, $j = 1 \text{ to } N$. The discretized values of $u(\tilde{x}_i, t_j)$ are denoted as u_i^j. By employing an implicit FDM scheme, which is unconditionally stable by von Neumann

4

stability analysis, the governing Eq.(1) is discretized as follows:

$$\frac{u_i^{j+1} - u_i^j}{\Delta t} = \frac{u_{i+1}^{j+1} - 2u_i^{j+1} + u_{i-1}^{j+1}}{(\Delta x)^2} + h^{j+1}g(u_i^{j+1}) + f_i^{j+1}, \quad i = \overline{1, M}, \ j = \overline{1, N-1}. \tag{5}$$

The nonlinear source term $g(u_i^{j+1})$ is linearized by a first-order Taylor series expansion [32, 45],

$$g(u_i^{j+1}) = g(u^*) + g'(u^*)(u_i^{j+1} - u^*), \tag{6}$$

and then Eq.(6) is substituted into Eq.(5) to obtain the following recurrence relationship:

$$\begin{aligned}
\left[1 + 2r - h^{j+1}g'(u^*)\Delta t\right] u_i^{j+1} - r u_{i+1}^{j+1} - r u_{i-1}^{j+1} \\
= u_i^j + \Delta t \left[h^{j+1}\left(g(u^*) - g'(u^*)u^*\right) + f_i^{j+1}\right],
\end{aligned} \tag{7}$$

where $r = \Delta t/(\Delta x)^2$, g' denotes the first derivative of g, and u^* is the previously iterated solution. The boundary conditions (2) and (3) can be discretized as follows:

$$\frac{u_0^{j+1} - u_2^{j+1}}{2\Delta x} = q^{j+1}, \quad j = \overline{1, N-1}, \tag{8}$$

$$\frac{u_{M+1}^{j+1} - u_{M-1}^{j+1}}{2\Delta x} = 0, \quad j = \overline{1, N-1}, \tag{9}$$

where u_0^{j+1} and u_{M+1}^{j+1} are nodal temperatures at fictitious points $i = 0$ and $i = M+1$ on the left-hand side and right-hand side of the boundaries $x = 0$ and $x = 1$, respectively. The fictitious nodal temperatures can be further eliminated by substituting Eqs.(8) and (9) into Eq.(5) for $i = 1$ and M. To solve Eq.(7), the iteration is implemented by assuming $u^* = u_i^j$, namely the values at previous time step. With these new values as better guesses, repeat the process until the changes in the values of u are negligible.

3. Inverse problem

In the inverse problem, both the time-dependent heat flux $q(t)$ and the reaction coefficient $h(t)$ are unknown and need to be determined together with the temperature $u(x, t)$. In this study, the time varying temperature measurements at two points $x = x_1$ and x_2 $(0 \leq x_2 < x_1 \leq 1)$, as shown in Figure 1, are taken as the overspecification needed to compensate for the missing information. For linear problems where $g(u) = u$, similar inverse problems have been widely considered in the literatures, see for instance [12, 25, 26, 41, 44] for the recovery of the blood perfusion coefficient $h(t)$, and [19] for the recovery of the heat flux $q(t)$. In the case $g(u) = u^\chi$ with $\chi \in (0, 1)$, the existence and uniqueness of the pair $(q(t), u(x, t))$ for the homogeneous heat equation (1) with homogeneous Neumann boundary conditions (2) and (3), initial condition (4) and internal measurement (12) with $0 < x_2 < 1$, was established in [34] and [4, Sect.7.2]. In our paper, in section 4 we will show for the first time the local (in time) existence and uniqueness of the pair solution $(h(t), u(x, t))$ satisfying Eqs.(11)-(15) with a general

5
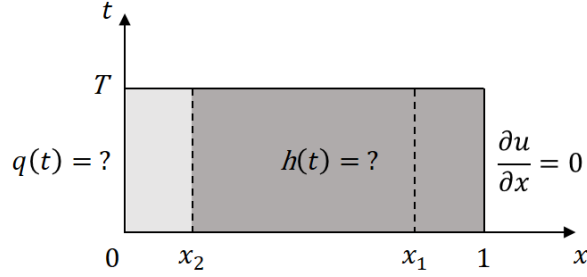
Figure 1. Schematic representation of the inverse problem considered.

nonlinear source term $g(u)$, when the first three derivatives of g are Lipschitz continuous functions. We also mention that some different inverse source problems where h depends on x, or where the function $g(u)$ is unknown have been investigated elsewhere, see [6, 13, 35, 42].

Considering the ill-posedness of the inverse problem, we formulate it in the framework of least-squares variational minimization. The unknown functions $h(t)$ and $q(t)$ are sought by solving two separate inverse problems described below.

The objective functions for minimization, which characterize the residual between the temperature measurement and the calculated value, are listed as follows:

$$\begin{cases} J_1[h(t)] = \frac{1}{2} \int_0^T [u(x_1, t; h) - Y_1(t)]^2 \, dt, \\ J_2[q(t)] = \frac{1}{2} \int_0^T [u(x_2, t; q) - Y_2(t)]^2 \, dt, \end{cases} \tag{10}$$

where Y_i are the measured temperatures at $x = x_i$, $i = 1, 2$, respectively. There are no bounds on the variables h and q that need to be imposed in the minimization of (10). We take time-dependent temperature measurements with two sensors at $x = x_i$, $i = 1, 2$, because there are two unknown functions dependent on time that have to be identified.

The first step is to estimate $h(t)$ by minimizing J_1, which can be achieved by solving the IHSP defined in the domain $(x, t) \in [x_2, 1] \times [0, T]$, as shown in Figure 1. The problem is stated as follows:

$$\frac{\partial u}{\partial t} = \frac{\partial^2 u}{\partial x^2} + h(t)g(u) + f(x, t), \quad (x, t) \in [x_2, 1] \times [0, T], \tag{11}$$

with a Dirichlet boundary condition at $x = x_2$ (the measured temperature is used as a boundary condition) and the insulation condition at $x = 1$, namely,

$$u(x_2, t) = Y_2(t), \quad t \in [0, T], \tag{12}$$

$$\frac{\partial u}{\partial x}(1, t) = 0, \quad t \in (0, T], \tag{13}$$

the initial condition

$$u(x, 0) = u_0(x), \quad x \in [x_2, 1], \tag{14}$$

6

and the additional condition

$$u(x_1, t) = Y_1(t), \quad t \in [0, T], \tag{15}$$

where u_0, Y_1 and Y_2 satisfy consistency conditions, namely, $u_0'(1) = 0$, $Y_1(0) = u_0(x_1)$ and $Y_2(0) = u_0(x_2)$. Whilst the above inverse problem given by equations (11)-(15) for recovering the reaction coefficient $h(t)$ can be easily formulated in multiple spatial dimensions, its mathematical analysis described in the next section cannot be readily extended and is deferred to a future work.

With $h(t)$ being determined, the second step is to estimate $q(t)$ by minimizing J_2 in Eq.(10). The problem is considered as an IHCP, which consists in the evaluation of the unknown heat flux $q(t)$ and the temperature $u(x, t)$ satisfying Eqs.(1), (3), (4) and (12).

4. Mathematical analysis of the IHSP

In this section, we prove the existence and uniqueness of a classical solution to the IHSP (11)-(15). First, since the boundary condition (12) is non-homogeneous, we introduce a new variable $v(\hat{x}, t) := u(x, t) - Y_2(t)$. Then, from Eqs.(11)-(15), it is easy to see that $v(\hat{x}, t)$ satisfies the following problem:

$$\frac{\partial v}{\partial t} = D\frac{\partial^2 v}{\partial \hat{x}^2} + h(t)g(v + Y_2(t)) + \hat{f}(\hat{x}, t), \quad (\hat{x}, t) \in D_T := [0, 1] \times [0, T], \tag{16}$$

$$v(0, t) = \frac{\partial v}{\partial \hat{x}}(1, t) = 0, \quad t \in (0, T], \tag{17}$$

$$v(\hat{x}, 0) = u_0(x) - Y_2(0) =: \varphi(\hat{x}), \quad \hat{x} \in [0, 1], \tag{18}$$

and the additional condition is

$$v(\hat{x}_1, t) = Y_1(t) - Y_2(t) =: a(t), \quad t \in [0, T], \tag{19}$$

where $D = \frac{1}{(1-x_2)^2}$, $\hat{x} = \frac{x-x_2}{1-x_2}$, $\hat{x}_1 = \frac{x_1-x_2}{1-x_2}$ and $\hat{f}(\hat{x}, t) = f(x, t) - Y_2'(t)$. The functions φ and a satisfy the consistency conditions $\varphi(0) = 0$ and $\varphi(\hat{x}_1) = a(0)$. The pair $(h(t), v(\hat{x}, t))$ from the class $C[0, T] \times C^{2,1}(D_T)$ which satisfies (16)-(19) is called a classical solution of the inverse problem (16)-(19).

We attempt to apply the Fourier method of eigenfunction expansion to the problem (16)-(19). Consider first the auxiliary spectral problem given by

$$\begin{cases} DX''(\hat{x}) + \Lambda X(\hat{x}) = 0, & \hat{x} \in [0, 1], \\ X(0) = X'(1) = 0, \end{cases} \tag{20}$$

which has the eigenvalues $\Lambda_n = D\mu_n^2$ and the eigenfunctions $X_n(\hat{x}) = \sin(\mu_n \hat{x})$, where $\mu_n = \left(\frac{\pi}{2} + n\pi\right)$ for $n = 0, 1, \ldots$.

Let us seek the solution of the problem (16)-(19) in the form

$$v(\hat{x}, t) = \sum_{n=0}^{\infty} v_n(t) \sin(\mu_n \hat{x}), \tag{21}$$

where $v_n(t)$ is the solution of the following initial value problem:

$$\begin{cases} v_n'(t) + D\mu_n^2 v_n(t) = F_n(t; v, h), \\ v_n(0) = \varphi_n. \end{cases} \tag{22}$$

Here $\varphi_n = 2\int_0^1 \varphi(\hat{x})\sin(\mu_n\hat{x})\,d\hat{x}$ and $F_n(t; v, h) = h(t)g_n(t) + f_n(t)$, where $g_n(t) = 2\int_0^1 g(v(\hat{x}, t) + Y_2(t))\sin(\mu_n\hat{x})\,d\hat{x}$ and $f_n(t) = 2\int_0^1 \hat{f}(\hat{x}, t)\sin(\mu_n\hat{x})\,d\hat{x}$. The solution of (22) satisfies the nonlinear integral equation

$$v_n(t) = \varphi_n e^{-D\mu_n^2 t} + \int_0^t F_n(s; v, h)e^{D\mu_n^2(s-t)}\,ds. \tag{23}$$

Substituting Eq.(23) into Eq.(21), we get

$$v(\hat{x}, t) = \sum_{n=0}^\infty \left[\varphi_n e^{-D\mu_n^2 t} + \int_0^t F_n(s; v, h)e^{D\mu_n^2(s-t)}\,ds \right] \sin(\mu_n\hat{x}). \tag{24}$$

Consider $\hat{x} = \hat{x}_1$ in Eq.(16) and use the over-specification condition (19) to obtain

$$h(t) = \frac{1}{g(a(t) + Y_2(t))} \left[a'(t) - \hat{f}(\hat{x}_1, t) + D\sum_{n=0}^\infty \mu_n^2 \sin(\mu_n\hat{x}_1)v_n(t). \right]. \tag{25}$$

The pair $z := [h(t), v(\hat{x}, t)]^{\mathrm{T}}$ satisfies the nonlinear system of equations (24) and (25), which can be rewritten as an operator equation

$$z = \Phi(z). \tag{26}$$

The operator Φ has the form $[\phi_0, \phi]^{\mathrm{T}}$, where

$$\phi_0(z) = \frac{1}{g(a(t) + Y_2(t))} \left[a'(t) - \hat{f}(\hat{x}_1, t) \right.$$
$$\left. + D\sum_{n=0}^\infty \mu_n^2 \sin(\mu_n\hat{x}_1) \left(\varphi_n e^{-D\mu_n^2 t} + \int_0^t F_n(s; v, h)e^{D\mu_n^2(s-t)}\,ds \right) \right], \tag{27}$$

$$\phi(z) = \sum_{n=0}^\infty \left[\varphi_n e^{-D\mu_n^2 t} + \int_0^t F_n(s; v, h)e^{D\mu_n^2(s-t)}\,ds \right] \sin(\mu_n\hat{x}). \tag{28}$$

One can note that Eq.(27) contains the derivative $a'(t)$ of the function $a(t) = Y_1(t) - Y_2(t)$ whose numerical differentiation represents an ill-posed problem since the data (12) and (15) come from measurement which is inherently contaminated with random noise.

Let us now introduce the functional space [23]

$$B_{2,T}^3 := \left\{ v(\hat{x}, t) = \sum_{n=0}^{\infty} v_n(t) \sin(\mu_n \hat{x}) : \ v_n(t) \in C[0, T], \right.$$

$$\left. J_T(v) := \left[\sum_{n=0}^{\infty} \left(\mu_n^3 \|v_n(t)\|_{C[0,T]} \right)^2 \right]^{1/2} < +\infty \right\}, \tag{29}$$

with the norm $\|v\|_{B_{2,T}^3} := J_T(v)$. It can be shown that $B_{2,T}^3$ is a Banach space. Obviously, $E_T^3 := B_{2,T}^3 \times C[0, T]$ with the norm $\|z\|_{E_T^3} = \|v(\hat{x}, t)\|_{B_{2,T}^3} + \|h(t)\|_{C[0,T]}$ is also a Banach space.

Let us show that Φ maps E_T^3 onto itself continuously. In other words, we need to show that $\phi_0(z) \in C[0, T]$ and $\phi(z) \in B_{2,T}^3$ for arbitrary $z = [h(t), v(\hat{x}, t)]^{\mathrm{T}}$, where $h(t) \in C[0, T]$ and $v(\hat{x}, t) \in B_{2,T}^3$.

We will use the following assumptions on the data of problem (16)-(19):

($\mathbf{A}_1$): $\varphi(\hat{x}) \in C^3[0, 1]$, $a(t) \in C^1[0, T]$, $\varphi(0) = \varphi'(1) = \varphi''(0) = 0$, $\varphi(\hat{x}_1) = a(0)$;

($\mathbf{A}_2$): $\hat{f}(\hat{x}, t) \in C(D_T)$, $\hat{f}(\cdot, t) \in C^3[0, 1]$, $\forall t \in [0, T]$, $\hat{f}(0, t) = \hat{f}_{\hat{x}}(1, t) = \hat{f}_{\hat{x}\hat{x}}(0, t) = 0$;

($\mathbf{A}_3$): $\begin{cases} Y_2(t) \in C^1[0, T], \ g(v) \in C^3(\mathbb{R}), \ g(Y_2(t)) = g'(Y_2(t)) = g''(Y_2(t)) = 0, \\ g(a(t) + Y_2(t)) \neq 0, \ \forall t \in [0, T]; g', \ g'' \text{ and } g''' \text{ are Lipschitz continuous} \\ \text{functions, i.e., there exist non-negative real constants } c_i, \ i = 1, 2, 3, \text{ such that} \\ |g'(v) - g'(w)| \leq c_1 |v - w|, \quad |g''(v) - g''(w)| \leq c_2 |v - w|, \\ |g'''(v) - g'''(w)| \leq c_3 |v - w|, \ \forall v, \ w \in \mathbb{R}. \end{cases}$

First, let us show that $\phi_0(z) \in C[0, T]$. Using integration by parts, it easy to see that using (17), the assumptions ($\mathbf{A}_1$), ($\mathbf{A}_2$) and first condition of ($\mathbf{A}_3$), we have

$$\begin{cases} \varphi_n = -\frac{2}{\mu_n^3} \int_0^1 \varphi'''(\hat{x}) \cos(\mu_n \hat{x}) \, d\hat{x}, \\ f_n(t) = -\frac{2}{\mu_n^3} \int_0^1 \hat{f}_{\hat{x}\hat{x}\hat{x}}(\hat{x}, t) \cos(\mu_n \hat{x}) \, d\hat{x}, \\ g_n(t) = -\frac{2}{\mu_n^3} \int_0^1 \left(g_{vvv} v_{\hat{x}}^3 + 3 g_{vv} v_{\hat{x}\hat{x}} v_{\hat{x}} + g_v v_{\hat{x}\hat{x}\hat{x}} \right) \cos(\mu_n \hat{x}) \, d\hat{x}, \end{cases} \tag{30}$$

From Eqs.(27) and (30), we obtain

$$|\phi_0(z)| \leq \frac{1}{|g(a(t) + Y_2(t))|} \left\{ |a'(t)| + |\hat{f}(\hat{x}_1, t)| \right.$$

$$\left. + \sum_{n=0}^{\infty} \frac{D}{\mu_n} \left[|\alpha_n| + \int_0^T \left(|h(t)| \, |\eta_n(t)| + |\gamma_n(t)| \right) dt \right] \right\}, \tag{31}$$

where

$$\begin{cases} \alpha_n := \mu_n^3 \varphi_n = -2 \int_0^1 \varphi'''(\hat{x}) \cos(\mu_n \hat{x}) \, d\hat{x}, \\ \eta_n(t) := \mu_n^3 g_n(t) = -2 \int_0^1 \left(g_{vvv} v_{\hat{x}}^3 + 3 g_{vv} v_{\hat{x}\hat{x}} v_{\hat{x}} + g_v v_{\hat{x}\hat{x}\hat{x}} \right) \cos(\mu_n \hat{x}) \, d\hat{x}, \\ \gamma_n(t) := \mu_n^3 f_n(t) = -2 \int_0^1 \hat{f}_{\hat{x}\hat{x}\hat{x}}(\hat{x}, t) \cos(\mu_n \hat{x}) \, d\hat{x}. \end{cases} \tag{32}$$

The majorizing series in (31) is convergent by using ($\mathbf{A}_1$)-($\mathbf{A}_3$) and the Cauchy-Schwartz and Bessel inequalities. This implies that by the Weierstrass-M test, the series in (27) is uniformly convergent in $[0, T]$. Thus, ϕ_0 is continuous in $[0, T]$.

9

Now, let us show that $\phi(z) \in B_{2,T}^3$, i.e. we need to show that

$$\left[\sum_{n=0}^{\infty}\left(\mu_n^3 \max_{0 \le t \le T} |\phi_n(t)|\right)^2\right]^{1/2} < +\infty, \tag{33}$$

where $\phi_n(t) := \varphi_n e^{-D\mu_n^2 t} + \int_0^t F_n(s;v,h)e^{D\mu_n^2(s-t)}ds$ by (28). Applying integration by parts, as before (e.g. as in (30)-(32)), we obtain

$$\phi_n(t) = \frac{1}{\mu_n^3}\left[\alpha_n e^{-D\mu_n^2 t} + \int_0^t [h(s)\eta_n(s) + \gamma_n(s)]e^{D\mu_n^2(s-t)}ds\right], \tag{34}$$

under the assumption $(\mathbf{A}_1)$-$(\mathbf{A}_3)$. This implies

$$\mu_n^3 |\phi_n(t)| \le |\alpha_n| + \int_0^T \left(|h(t)||\eta_n(t)| + |\gamma_n(t)|\right) dt. \tag{35}$$

From the inequality (35), we obtain

$$\sum_{n=0}^{\infty}\left(\mu_n^3 \max_{0 \le t \le T} |\phi_n(t)|\right)^2 \le 2\sum_{n=0}^{\infty}|\alpha_n|^2$$
$$+ 4T^2\left[\left(\max_{0 \le t \le T} |h(t)|\right)^2 \sum_{n=0}^{\infty}\max_{0 \le t \le T}|\eta_n(t)|^2 + \sum_{n=0}^{\infty}\max_{0 \le t \le T}|\gamma_n(t)|^2\right]. \tag{36}$$

From the Bessel inequality, the series on the right hand side of (36) are convergent. Thus, $J_T(\phi) < +\infty$ and thus ϕ belongs to the space $B_{2,T}^3$.

Let us now show that Φ is a contraction mapping on E_T^3. Let $z_1 = [h(t), v(\hat{x},t)]^{\mathrm{T}}$ and $z_2 = [\tilde{h}(t), \tilde{v}(\hat{x},t)]^{\mathrm{T}}$ be any two elements of E_T^3. We know that $\|\Phi(z_1) - \Phi(z_2)\|_{E_T^3} = \|\phi_0(z_1) - \phi_0(z_2)\|_{C[0,T]} + \|\phi(z_1) - \phi(z_2)\|_{B_{2,T}^3}$.

After applying integration by parts to Eqs.(27) and (28), under the assumptions $(\mathbf{A}_1)$-$(\mathbf{A}_2)$ and first part of $(\mathbf{A}_3)$, we obtain

$$\phi_0(z_1) - \phi_0(z_2) = \frac{-D}{g(a(t) + Y_2(t))}\left[\sum_{n=0}^{\infty}\frac{2}{\mu_n}\sin(\mu_n \hat{x}_1)\int_0^t M(h,\tilde{h},v,\tilde{v})e^{D\mu_n^2(s-t)}ds\right], \tag{37}$$

$$\phi(z_1) - \phi(z_2) = -\sum_{n=0}^{\infty}\frac{2}{\mu_n^3}\sin(\mu_n \hat{x}_1)\int_0^t M(h,\tilde{h},v,\tilde{v})e^{D\mu_n^2(s-t)}ds, \tag{38}$$

where

$$M(h,\tilde{h},v,\tilde{v}) := h(s)\int_0^1 \left[g_{vvv}v_{\hat{x}}^3 + 3g_{vv}v_{\hat{x}\hat{x}}v_{\hat{x}} + g_v v_{\hat{x}\hat{x}\hat{x}}\right]\cos(\mu_n \hat{x})\,d\hat{x}$$
$$-\tilde{h}(s)\int_0^1 \left[g_{vvv}\tilde{v}_{\hat{x}}^3 + 3g_{vv}\tilde{v}_{\hat{x}\hat{x}}\tilde{v}_{\hat{x}} + g_v \tilde{v}_{\hat{x}\hat{x}\hat{x}}\right]\cos(\mu_n \hat{x})\,d\hat{x}. \tag{39}$$

10

By using the Cauchy-Schwartz inequality from (21) it is easy to obtain that

$$|v_{\hat{x}}| = \left| \sum_{n=0}^{\infty} \mu_n v_n(t) \cos(\mu_n \hat{x}) \right| \leq \sum_{n=0}^{\infty} \frac{1}{\mu_n^2} \left(\mu_n^3 \max_{0 \leq t \leq T} |v_n(t)| \right) \leq c \, \|v\|_{B_{2,T}^3}, \quad (40)$$

$$|v_{\hat{x}\hat{x}}| = \left| -\sum_{n=0}^{\infty} \mu_n^2 v_n(t) \sin(\mu_n \hat{x}) \right| \leq \sum_{n=0}^{\infty} \frac{1}{\mu_n} \left(\mu_n^3 \max_{0 \leq t \leq T} |v_n(t)| \right) \leq c \, \|v\|_{B_{2,T}^3}, \quad (41)$$

$$\int_0^1 v_{\hat{x}\hat{x}\hat{x}}^2 \, d\hat{x} = \left(-\sum_{n=0}^{\infty} \mu_n^3 v_n(t) \cos(\mu_n \hat{x}), \ -\sum_{n=0}^{\infty} \mu_n^3 v_n(t) \cos(\mu_n \hat{x}) \right)_{L_2[0,1]}$$

$$= \frac{1}{2} \sum_{n=0}^{\infty} \left(\mu_n^3 |v_n(t)| \right)^2 \leq \frac{1}{2} \|v\|_{B_{2,T}^3}^2, \quad (42)$$

where $(\cdot, \cdot)_{L_2(0,1)}$ denotes the inner product in $L_2(0,1)$, $c = \left[\sum_{n=0}^{\infty} \frac{1}{\mu_n^2} \right]^{\frac{1}{2}}$, and similar inequalities for $\tilde{v}$.

After some manipulations in Eqs.(37) and (38) and using the estimates (40)-(42) and the Lipschitz continuities in $(\mathbf{A}_3)$, we obtain

$$\|\Phi(z_1) - \Phi(z_2)\|_{E_T^3} \leq A(T) C(h, \tilde{h}, v, \tilde{v}) \|z_1 - z_2\|_{E_T^3}, \quad (43)$$

where $A(T) := \sqrt{T} \left(1 + \left\| \frac{D}{g(a(t) + Y_2(t))} \right\|_{C[0,T]} \right)$ and $C(h, \tilde{h}, v, \tilde{v})$ is a positive constant dependent on some multiplications and summations of the norms of $\|h\|_{C[0,T]}$, $\|\tilde{h}\|_{C[0,T]}$, $\|v\|_{B_{2,T}^3}^2$ and $\|\tilde{v}\|_{B_{2,T}^3}^2$.

Since $A(T)$ has limit zero as T tends to zero, it means that, for sufficient small T, the operator Φ is contraction mapping which maps E_T^3 onto itself continuously. Then according to Banach fixed point theorem there exists unique solution to Eq.(26) in E_T^3.

Thus, we have proved the following theorem:

Theorem 4.1. *Let the assumptions $(\mathbf{A}_1)$-$(\mathbf{A}_3)$ be satisfied. Then, the inverse problem (16)-(19) has a unique classical solution $(v(\hat{x}, t), h(t)) \in E_T^3$ for small T. Moreover, $v(\hat{x}, t) \in C^{2,1}(D_T)$.*

The fact that $v(\hat{x}, t)$ also belongs to $C^{2,1}(D_T)$ follows noting that from (29) we have $v_{\hat{x}\hat{x}}(\hat{x}, t) \in C(D_T)$, from $(\mathbf{A}_2)$ we have that $\hat{f}(\hat{x}, t) \in C(D_T)$, from $(\mathbf{A}_3)$ it results that $g(v(\hat{x}, t) + Y_2(t)) \in C(D_T)$ and also since $h \in C(D_T)$ from (16) we obtain that $v_t(\hat{x}, t) \in C(D_T)$.

Noting that $Y_1(t) = a(t) + Y_2(t)$, $u(x, t) = v(\hat{x}, t) + Y_2(t)$, $u_0(x) = \varphi(\hat{x}) + Y_2(0)$, and $f(x, t) = \hat{f}(\hat{x}, t) + Y_2'(t)$, where $\hat{x} = \frac{x - x_2}{1 - x_2}$, then under the following assumptions:

$(\mathbf{A}_1')$: $u_0 \in C^3[x_2, 1]$, $Y_1 \in C^1[0, T]$, $Y_2 \in C^1[0, T]$, $u_0(x_2) = Y_2(0)$, $u_0'(1) = u_0''(0) = 0$, $u_0(x_1) = Y_1(0)$;

$(\mathbf{A}_2')$: $f(x, t) \in C([x_2, 1] \times [0, T])$, $f(\cdot, t) \in C^3[x_2, 1]$, $\forall t \in [0, T]$, $f(x_2, t) = Y_2'(t)$, $f_x(1, t) = f_{xx}(x_2, t) = 0$;

$(\mathbf{A}_3')$: The same as $(\mathbf{A}_3)$, but with the condition $g(a(t) + Y_2(t)) \neq 0$, $\forall t \in [0, T]$ being replaced by the condition $g(Y_1(t)) \neq 0$, $\forall t \in [0, T]$,

it follows that the original IHSP (11)-(15) has a unique classical solution $(u(x,t), h(t)) \in \tilde{B}_{2,T}^3 \times C[0,T]$ for small T, where

$$\tilde{B}_{2,T}^3 := \left\{ u(x,t) = Y_2(t) + v(\hat{x}, t) : v(\hat{x}, t) \in B_{2,T}^3 \cap C^{2,1}(D_T) \right\} \subset C^{2,1}(D_T). \quad (44)$$

5. The numerical procedure based on CGM

The estimations of $h(t)$ and $q(t)$, as minimizers of (10), can be achieved either by gradient-free heuristic techniques, such as evolutionary optimization algorithms [9–11, 17], or by gradient-based methods. Gradient-free methods can be applied to problems where the objective function is not differentiable, but if this is not the case, gradient-based deterministic techniques are preferred due to their higher efficiency. In this study, the rigorous CGM is applied for the numerical optimization of least-squares functional. Assuming that $P(t)$ is the function needed to be estimated, the value of $P(t)$ at iteration $n + 1$ is

$$P^{n+1}(t) = P^n(t) - \beta^n d^n(t), \quad n = 0, 1, \ldots, \quad (45)$$

where the superscript n is the number of iteration, P^0 is an initial guess, β^n is the search step size and d^n is the direction of descent given by:

$$d^0(t) = J'[P^0], \quad d^n(t) = J'[P^n] + \gamma^n d^{n-1}(t), \quad n = 1, 2, \ldots, \quad (46)$$

where J stands for J_1 or J_2 in (10) depending on whether $h(t)$ or $q(t)$ is estimated, respectively. The conjugate coefficient γ^n is calculated by the Polak-Ribiere expression, [2],

$$\gamma^n = \frac{\int_0^T J'[P^n] \left(J'[P^n] - J'[P^{n-1}] \right) dt}{\int_0^T \left(J'[P^{n-1}] \right)^2 dt}, \quad n = 1, 2, \ldots. \quad (47)$$

Here, the gradient $J'[P^n]$ can be derived from the solution of an adjoint problem, which will be presented in section 5.2. Further, the search step size β^n is found by minimizing the function $J[P^n - \beta^n d^n]$ with respect to β^n, and following a similar analysis to that of [7] we obtain

$$\beta^n = \frac{\int_0^T [u(t; P^n) - Y(t)] \Delta u^n dt}{\int_0^T (\Delta u^n)^2 dt}, \quad n = 0, 1, \ldots, \quad (48)$$

where $\Delta u^n = \Delta u(t; d^n)$ is obtained by solving the sensitivity problem (49) or (50) by setting $\Delta P^n = d^n$, [1].

5.1. The sensitivity problem

Consider first the estimation of $h(t)$. The sensitivity problem is obtained from the direct problem by adding a perturbation $\varepsilon \Delta h(t)$ to $h(t)$, and the subsequent response $u_h(x,t)$ is perturbed by $\varepsilon \Delta u_h(x,t)$, where ε is a small parameter. The increment

$\Delta u_h(x,t)$ satisfies the following sensitivity problem:

$$\begin{cases} \frac{\partial \Delta u_h}{\partial t} = \frac{\partial^2 \Delta u_h}{\partial x^2} + h(t)g'(u_h(x,t))\Delta u_h + g(u_h)\Delta h, & (x,t) \in [x_2,1] \times [0,T], \\ \Delta u_h(x_2,t) = 0, \quad \frac{\partial}{\partial x}\Delta u_h(1,t) = 0, & t \in (0,T], \\ \Delta u_h(x,0) = 0, & x \in [x_2,1]. \end{cases} \quad (49)$$

Now consider the sensitivity problem of estimating $q(t)$. The increment $\Delta u_q(x,t)$ resulted from the perturbation $\varepsilon \Delta q(t)$ is the solution of the following sensitivity problem,

$$\begin{cases} \frac{\partial \Delta u_q}{\partial t} = \frac{\partial^2 \Delta u_q}{\partial x^2} + h(t)g'(u_q(x,t))\Delta u_q, & (x,t) \in [0,1] \times [0,T], \\ \frac{\partial}{\partial x}\Delta u_q(0,t) = -\Delta q(t), \quad \frac{\partial}{\partial x}\Delta u_q(1,t) = 0, & t \in (0,T], \\ \Delta u_q(x,0) = 0, & x \in [0,1]. \end{cases} \quad (50)$$

5.2. The adjoint problem

Because the temperature appearing in the objective function (10) needs to satisfy the direct problem, we consider the following constrained objective functional for $h(t)$ by introducing a Lagrange multiplier $\lambda_h(x,t)$:

$$\begin{aligned} J_1[h] =& \frac{1}{2} \int_0^T \int_{x_2}^1 [u_h(x,t;h) - Y_1(t)]^2 \, \delta(x-x_1) \, dxdt \\ &+ \int_0^T \int_{x_2}^1 \lambda_h(x,t) \left[\frac{\partial^2 u_h}{\partial x^2} + h(t)g(u_h) + f(x,t) - \frac{\partial u_h}{\partial t} \right] dxdt, \end{aligned} \quad (51)$$

where δ is the Dirac delta function. The first variation, $\Delta J_1[h] = J_1[h + \Delta h] - J_1[h]$, of the objective function $J_1[h]$ is derived as follows:

$$\begin{aligned} \Delta J_1[h] =& \int_0^T \int_{x_2}^1 \Delta u_h [u_h(x,t) - Y_1(t)]\delta(x-x_1) \, dxdt \\ &+ \int_0^T \int_{x_2}^1 \lambda_h(x,t) \left[\frac{\partial^2 \Delta u_h}{\partial x^2} + h(t)g'(u_h)\Delta u_h + g(u_h)\Delta h - \frac{\partial \Delta u_h}{\partial t} \right] dxdt \\ =& \int_0^T \int_{x_2}^1 \lambda_h g(u_h)\Delta h \, dxdt \\ &+ \int_0^T \left[\lambda_h \frac{\partial \Delta u_h}{\partial x}\Big|_{x_2}^1 - \Delta u_h \frac{\partial \lambda_h}{\partial x}\Big|_{x_2}^1 \right] dt - \int_{x_2}^1 \lambda_h \Delta u_h|_0^T \, dx \\ &+ \int_0^T \int_{x_2}^1 \Delta u_h \left[\frac{\partial^2 \lambda_h}{\partial x^2} + \frac{\partial \lambda_h}{\partial t} + \lambda_h h(t)g'(u_h) + (u_h - Y_1)\delta(x-x_1) \right] dxdt. \end{aligned} \quad (52)$$

Vanishing $\Delta J_1[h]$, the adjoint problem that governs the Lagrange multiplier $\lambda_h(x,t)$

13

is given by

$$
\begin{cases}
\frac{\partial \lambda_h}{\partial t} = -\frac{\partial^2 \lambda_h}{\partial x^2} - \lambda_h h(t) g'(u_h(x,t)) - (u_h - Y_1)\delta(x - x_1), & (x,t) \in [x_2, 1] \times [0,T], \\
\lambda_h(x_2, t) = 0, \quad \frac{\partial \lambda_h}{\partial x}(1,t) = 0, & t \in (0,T], \\
\lambda_h(x,T) = 0, & x \in [x_2, 1].
\end{cases}
\tag{53}
$$

The gradient formula of the functional $J_1[h]$ can then be obtained as

$$
J_1'[h] = \int_{x_2}^{1} \lambda_h(x,t) g(u_h(x,t))\, dx.
\tag{54}
$$

From Eq.(54) and the third equation in (53), one remarks that $J_1'[h]$ vanishes at the final time $t = T$. Similarly, the adjoint problem for to the estimation of $q(t)$ is given by

$$
\begin{cases}
\frac{\partial \lambda_q}{\partial t} = -\frac{\partial^2 \lambda_q}{\partial x^2} - \lambda_q h(t) g'(u_q(x,t)) - (u_q - Y_2)\delta(x - x_2), & (x,t) \in [0,1] \times (0,T], \\
\frac{\partial \lambda_q}{\partial x}(0,t) = 0, \quad \frac{\partial \lambda_q}{\partial x}(1,t) = 0, & t \in (0,T], \\
\lambda_q(x,T) = 0, & x \in [0,1].
\end{cases}
\tag{55}
$$

The subsequent gradient formula is

$$
J_2'[q] = \lambda_q(0,t),
\tag{56}
$$

which also vanishes at $t = T$.

5.3. Stopping criterion

Due to the ill-posedness of inverse problem, small random errors inherently present in the measured temperatures can cause large oscillations in the inverse solution. In order to illustrate the effect of measurement noise on the stablity of inverse solution, the temperature measurements are numerically simulated by adding random noise to the exact $Y_i(t) = u(x_i, t)$, as

$$
Y_i^{\text{noise}}(t) = Y_i(t) + \epsilon_i(t), \quad i = 1,2,
\tag{57}
$$

where $\epsilon_i(t)$ is the measurement noise at $x = x_i$, satisfying a normal distribution with zero mean and standard deviation σ_i given by

$$
\sigma_i = p \times \max_{t \in [0,T]} |u(x_i, t)|, \quad i = 1,2,
\tag{58}
$$

where p represents the percentage of noise.

To stabilize the problem, the discrepancy principle is used for stopping the iterative procedure of the CGM, namely, cease the iteration at the first iteration number k for which

$$
J_i[P^k] \le \mathcal{E}_i, \quad i = 1,2,
\tag{59}
$$

where, from Eqs.(10) and (57),

$$\mathcal{E}_i = \frac{1}{2} \int_0^T \epsilon_i^2(t)\, dt, \quad i = 1, 2. \tag{60}$$

5.4. CGM algorithm

1). Choose an initial guess of $h^0(t)$ and set $n = 0$.
2). Solve the direct problem (Eqs.(11)-(14)) to obtain $u_h^n = u_h(x, t; h^n)$, and calculate $J_1[h^n]$. If $J_1[h^n]$ satisfies the stopping criterion (59), then go to step 6, else go to step 3.
3). Solve the adjoint problem (Eq.(53)) to calculate $\lambda_h(x, t; h^n)$, and the gradient $J_1'[h^n]$ by Eq.(54). Calculate the conjugate coefficient γ^n by Eq.(47) and the direction of descent d^n by Eq.(46).
4). Solve the sensitivity problem (Eq.(49)) to obtain $\Delta u_h(x, t; h^n)$ with $\Delta h^n = d^n$, and then calculate the search step size β^n using Eq.(48).
5). Obtain $h^{n+1}(t)$ via Eq.(45). If $J_1[h^{n+1}]$ satisfy the stopping criterion (59), then go to step 6, else set $n = n + 1$ and go to step 2.
6). Choose an initial guess of $q^0(t)$ and set $n = 0$.
7). Solve the direct problem (Eqs.(1)-(4)) to obtain $u_q^n = u_q(x, t; q^n)$, and calculate $J_2[q^n]$.
8). Solve the adjoint problem (Eq.(55)) and obtain the gradient $J_2'[q^n]$ by Eq.(56). Calculate γ^n and d^n.
9). Solve the sensitivity problem (Eq.(50)) and then calculate the search step size β^n.
10). Obtain $q^{n+1}(t)$ from Eq.(45). If $J_2[q^{n+1}]$ satisfy the stopping criterion, then stop the iteration (59), else set $n = n + 1$ and go to step 7.

6. Numerical results and discussion

In this section, we perform numerical experiments to validate the CGM in solving the inverse problem of determining $h(t)$ and afterwards $q(t)$. Two different functional forms of $g(u)$, $h(t)$ and $q(t)$ are tested here. To illustrate the accuracy of the inverse solution, the retrieved functions $h(t)$ and $q(t)$ are compared with the exact one $h_{\text{ext}}(t)$ and $q_{\text{ext}}(t)$. We define the accuracy errors at the iteration number n as

$$\begin{cases} E_1[h^n] = \sqrt{\frac{1}{N} \sum_{j=1}^N [h^n(t_j) - h_{\text{ext}}(t_j)]^2}, \\ E_2[q^n] = \sqrt{\frac{1}{N} \sum_{j=1}^N [q^n(t_j) - q_{\text{ext}}(t_j)]^2}. \end{cases} \tag{61}$$

A uniform grid is used to discretize the space ($x \in [0, 1]$) and time ($t \in [0, T = 1]$) domains. The integrals involved are approximated using the trapezium rule. In each example, both noiseless and noisy temperature data will be used for estimation to illustrate the accuracy and stability of the inverse solutions obtained by CGM.

6.1. Example 1

Let $T = 1$ and the functions in Eqs.(1)-(4) be as follows:

$$g(u) = \sin^3(u), \quad u_0(x) = \sin\left(\frac{\pi}{2} \cdot \frac{x - x_2}{1 - x_2}\right),$$

$$f(x, t) = \left(\frac{\pi^2}{4(1 - x_2)^2} - 1\right) \sin\left(\frac{\pi}{2} \cdot \frac{x - x_2}{1 - x_2}\right) e^{-t}$$

$$+ (1 + t^2) \sin^3\left(\sin\left(\frac{\pi}{2} \cdot \frac{x - x_2}{1 - x_2}\right) e^{-t}\right), \tag{62}$$

$$h(t) = -1 - t^2, \tag{63}$$

$$q(t) = -\frac{\pi}{2(1 - x_2)} \cos\left(\frac{\pi x_2}{2(1 - x_2)}\right) e^{-t}. \tag{64}$$

The analytical solution of the direct problem (1)-(4) is

$$u_{\text{ext}}(x, t) = \sin\left(\frac{\pi}{2} \cdot \frac{x - x_2}{1 - x_2}\right) e^{-t}. \tag{65}$$

Let us take $x_2 = 0.1$.

6.1.1. Direct problem (1)-(4)

The numerical solution of the direct Neumann problem given by Eqs.(1)-(4) is obtained using the iterative FDM described in section 2. In order to demonstrate the accuracy and convergence of the direct problem solution, we introduce the root mean square error (RMSE) defined as

$$\text{RMSE} = \sqrt{\frac{1}{N} \sum_{i=1}^{N} (u_{\text{num}}(x_1, t_i) - u_{\text{ext}}(x_1, t_i))^2}, \tag{66}$$

where, for simplicity, only the result at $x = x_1 = 0.9$ is used for evaluation and $u_{\text{num}}(x_1, t)$ denotes the numerical solution at $x = x_1$. The RMSEs for various mesh sizes at different iteration numbers are presented in Table 1. It can be remarked that the solution converges after 2 iterations for all mesh sizes. Thus, the number of iterations in the direct problem solver for the following calculations is set to be 2. It can also be concluded that the accuracy improves, as the mesh size increases. In addition, it can be seen that the independence of mesh has been achieved and the mesh $\Delta t = 0.01$ and $\Delta x = 0.01$, i.e., $M = N = 101$, is sufficiently fine for accurately solving the direct problem.
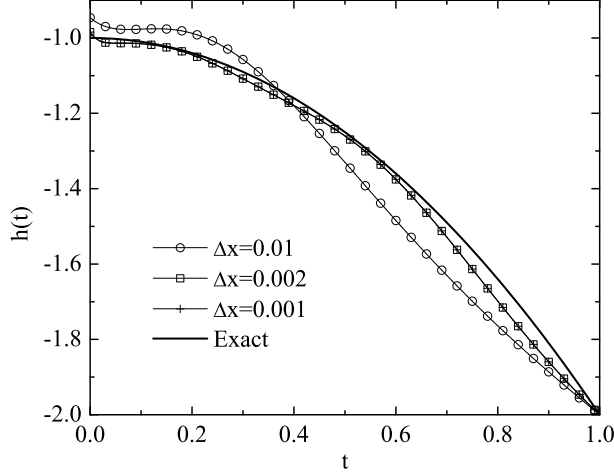
6.1.2. Inverse problem (11)-(15) of finding $h(t)$

For the inverse problem (11)-(15), the temperatures (12) and (15) given by

$$u(x_i, t) = \sin\left(\frac{\pi}{2} \cdot \frac{x_i - x_2}{1 - x_2}\right) e^{-t} = Y_i(t), \quad i = 1, 2, \tag{67}$$

Table 1. The RMSE of converged solution of the direct problem given by Eqs.(1)-(4) of example 1, obtained by the iterative FDM.

Iteration	$\Delta t = 0.1$ $\Delta x = 0.1$	$\Delta t = 0.05$ $\Delta x = 0.05$	$\Delta t = 0.01$ $\Delta x = 0.01$
1	1.0E-2	5.1E-3	1.0E-3
2	9.2E-3	4.9E-3	1.0E-3
3	9.2E-3	4.9E-3	1.0E-3

Figure 2. The inverse solution of $h(t)$ for noiseless data (15) at $x = x_1 = 0.9$ and (12) at $x = x_2 = 0.1$ for various space mesh sizes, for example 1. The time step is kept fixed at $\Delta t = 0.01$.

are taken as the noiseless measurement data. Remark that for (11), the temperature (12) at $x = x_2$ is in fact a Dirichlet boundary condition. Further, using Eqs.(18) and (19), we have

$$\varphi(\hat{x}) = u_0(\hat{x}) - Y_2(0) = \sin\left(\frac{\pi}{2}\hat{x}\right), \quad a(t) = Y_1(t) - Y_2(t) = \sin\left(\frac{\pi}{2}\hat{x}_1\right)e^{-t}, \quad (68)$$

which satisfy assumption ($\mathbf{A}_1$). Also, using the data (62), we obtain that

$$\hat{f}(\hat{x}, t) = f(x, t) - Y_2'(t) = \left(\frac{\pi^2}{4(1-x_2)^2} - 1\right)e^{-t}\sin\left(\frac{\pi}{2}\hat{x}\right)$$
$$+ (1 + t^2)\sin^3\left(e^{-t}\sin\left(\frac{\pi}{2}\hat{x}\right)\right), \quad (69)$$

which satisfies assumption ($\mathbf{A}_2$). Finally, $g(u) = \sin^3(u)$ satisfies assumption ($\mathbf{A}_3$). Then, according to Theorem 1, the inverse problem (11)-(15) has a unique (local) solution. In fact, this analytical solution is given by (63) and (65). The initial guess for the function $h(t)$ in the step 1 of the CGM algorithm described in section 5.4 is taken as

$$h^0(t) = -1 - t, \quad (70)$$

which matches the analytical solution (63) at the endpoints $t = 0$ and $t = T = 1$, but is sufficiently far from it otherwise.

17
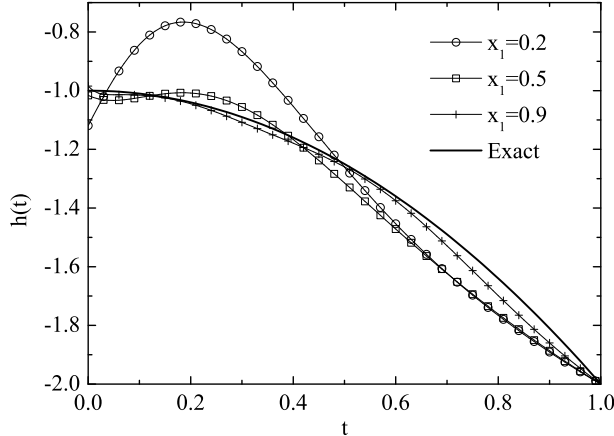
Figure 3. The inverse solution of $h(t)$ for noiseless data (12) at $x = x_2 = 0.1$ and (15) at various locations $x_1 \in \{0.2, 0.5, 0.9\}$, for example 1.

First, for a fixed time step $\Delta t = 0.01$ we investigate the influence of the space step Δx on the accuracy of the CGM numerical results for $h(t)$, as illustrated in Figure 2. From this figure it can be seen that the curves for $\Delta x = 0.002$ and $\Delta x = 0.001$ are overlapped. Thus, convergent results to the exact solution (63) are obtained, as Δx decreases to 0.002 and moreover, independence of this space mesh is achieved. In the next Figures 3-5 we present results obtained with the FDM mesh $\Delta t = 0.01$ and $\Delta x = 0.002$.

In Figure 3 we illustrate the behaviour of the numerically retrieved solution with respect to the location of the internal measurement $x = x_1$ inside the space solution domain $(x_2 = 0.1, 1)$. From this figure, it can be seen that the accuracy improves as x_1 approaches the boundary $x = 1$. Thus, for optimal design the sensor $x = x_2$ must be placed close to the boundary $x = 0$ where the unknown heat flux (2) is exerted, whilst the sensor $x = x_1$ should be placed close to the insulated boundary $x = 1$ where the zero heat flux condition (13) applies.

As shown in Figure 4(a), the objective function $J_1[h^n]$ that is minimized in Eq.(10) decreases monotonically, as a function of the iteration number n, for $p \in \{0, 1\%, 5\%\}$ noise. In the case of noisy data, the horizontal lines represent the thresholds determined from Eq.(60) for $i = 1$. The intersections of the horizontal lines with the curves of $J_1[h^n]$ yield the stopping iteration numbers, $n_h \in \{2, 1\}$ for $p \in \{1\%, 5\%\}$. These discrepancy principle stopping iteration numbers are in good agreement with the optimal ones which can be inferred from Figure 4(b), where the accuracy error $E_1[h^n]$ is plotted (for illustration only).

The solutions for $h(t)$ are illustrated in Figure 5 for $p \in \{0, 1\%, 5\%\}$ noise. The result is presented after 50 iterations for noiseless data $(p = 0)$, whilst for noisy data the results are presented for the stopping iteration number given by the stopping criterion (59) for $i = 1$, i.e., $n_h = 2$ iterations for $p = 1\%$ noise and $n_h = 1$ iteration for $p = 5\%$ noise. The numerical solution for $p = 0$ is in good agreement with the exact solution (63). Although the numerical solutions deviate from the exact solution (63) when the noise increases from $p = 1\%$ to $p = 5\%$, these are reasonably stable. Further, the accuracy improves as the percentage of noise p decreases.
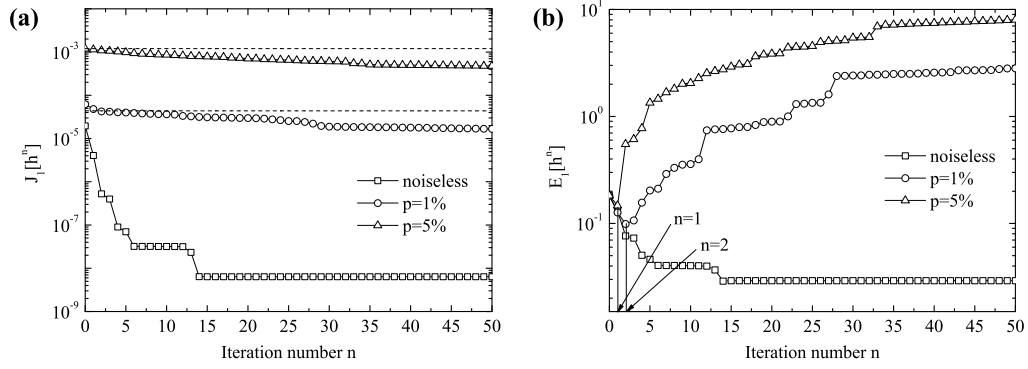
Figure 4. The evolution of (a) the objective function $J_1[h^n]$ and (b) the accuracy error $E_1[h^n]$, as functions of the iteration number n, for $p \in \{0, 1\%, 5\%\}$ noise, for example 1.
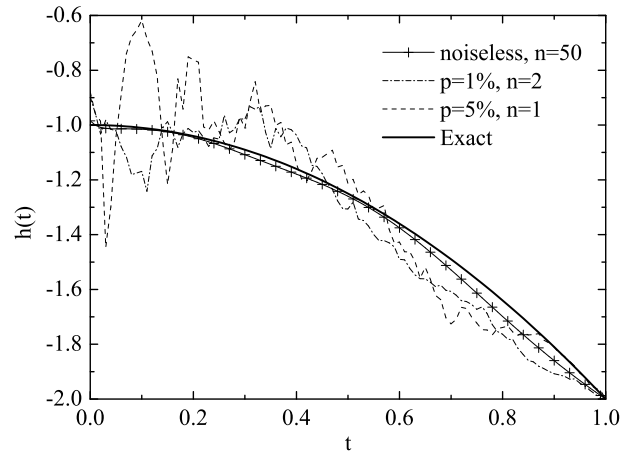
Figure 5. The inverse solution of $h(t)$, for $p \in \{0, 1\%, 5\%\}$ noise, for example 1.

19

6.1.3. Inverse problem (1), (3), (4) and (12) of finding q(t)

For the inverse problem (1), (3), (4) and (12), the uniqueness of solution is yet to be established although it is worth mentioning the recent investigation of [43] concerning the regularization of the sideways semilinear heat equation (1). We take the initial guess for $q(t)$ the linear function,

$$q^0(t) = \frac{\pi}{2(1-x_2)} \cos\left(\frac{\pi x_2}{2(1-x_2)}\right) \left[(1 - e^{-1}) t - 1\right], \tag{71}$$

which also matches the exact solution (64) at the endpoints $t = 0$ and $t = T = 1$, but is still reasonably far away from it. The temperature (67) at $x = x_2$, namely,

$$u(x_2, t) = Y_2(t) = 0, \tag{72}$$

is the internal measurement. Since, in this case, the measurement (72) models a zero temperature, it is not very realistic to add noise to it. Moreover, using (72) as input data instead of the numerical FDM solution $u(x_2, t)$ of the direct problem (1)-(4) (which has been obtained to be close to but not exactly equal to 0), avoids committing an inverse crime as well as simulating some numerically noisy data. The retrieved numerical solution of $q(t)$ has been found in very close agreement with the exact solution (64) and therefore these results are not presented (more on those in the next example 2).

6.2. Example 2

Many physical problems, such as spontaneous ignition [45], polymerization [22] and pyrolysis [33], are known to be governed by the transient diffusion equation with a highly nonlinear reaction-heating term. By employing the Frank-Kamenetskii approximation, the reaction-heating term can be simplified into an exponential function of temperature, which has a higher non-linearity than the power law relationship encountered in microwave heating [45]. Therefore, in this example, we take

$$g(u) = e^u, \quad f(x, t) = \frac{\pi}{2} \sin\left(\frac{\pi x}{2}\right) e^{-t}, \quad u_0(x) = \frac{2}{\pi} \sin\left(\frac{\pi x}{2}\right). \tag{73}$$

The input data in Eq.(73) do not satisfy some of the assumptions $(\mathbf{A}_1)$-$(\mathbf{A}_3)$, so we cannot conclude on the unique solvability of the inverse problem (11)-(15) for finding the reaction coefficient $h(t)$. Moreover, in contrast to the previous example which contained smooth functions (63) and (64), in this example we consider retrieving the discontinuous step functions,

$$h(t) = \begin{cases} 0, & t \in [0, 0.25), \\ -1, & t \in [0.25, 0.75), \\ 0, & t \in [0.75, 1], \end{cases} \tag{74}$$

$$q(t) = \begin{cases} -1, & t \in [0, 0.5), \\ 0, & t \in [0.5, 1]. \end{cases} \tag{75}$$

In this case, the direct problems given by Eqs.(1)-(4) and Eqs.(11)-(14) do not have analytical solutions for the temperature function $u(x, t)$. Hence, the input temperatures
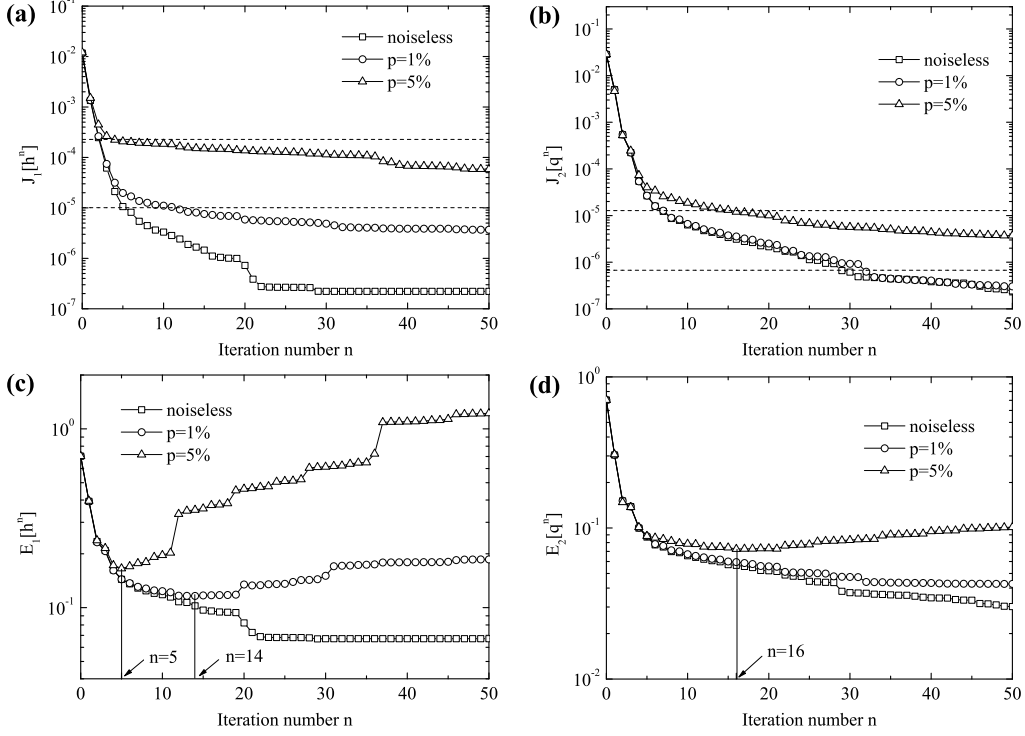
Figure 6. The evolution of the objective functions (a) $J_1[h^n]$ and (b) $J_2[q^n]$, and the accuracy errors (c) $E_1[h^n]$ and (d) $E_2[q^n]$, as functions of the iteration number n, for $p \in \{0, 1\%, 5\%\}$ noise, for example 2.

(12) and (15) for the inverse problem are numerically simulated by solving the direct problem given by Eqs.(1)-(4) with the input functions given by Eqs.(73)-(75).

Let us take $x_2 = 0.1$, $x_1 = 0.5$, and the initial guesses $h^0(t) = q^0(t) = 0$. In the following Figures 6 and 7, numerical results obtained with the FDM mesh $\Delta t = 0.01$ and $\Delta x = 0.002$ for various percentages of noise $p \in \{0, 1\%, 5\%\}$ are presented.

Figures 6(a) and 6(b) show the monotonic decrease convergences of the objective functions $J_1[h^n]$ and $J_2[q^n]$, as functions of the iteration number n. For noisy data, the horizontal lines determined from Eq.(60) intersect with the curves of $J_1[h^n]$ and $J_2[q^n]$, yielding the stopping iteration numbers $n_h \in \{12, 4\}$ and $n_q \in \{32, 16\}$ for $p \in \{1\%, 5\%\}$ noise, respectively, according to the discrepancy principle (59). Besides, the optimal iteration numbers minimizing the accuracy errors $E_1[h^n]$ and $E_2[q^n]$ are obtained as $n_{\text{opt},h} \in \{14, 5\}$ and $n_{\text{opt},q} \in \{50, 16\}$ for $p \in \{1\%, 5\%\}$ noise, as shown in Figures 6(c) and 6(d), respectively, for illustration only. The stopping iteration numbers n_h and n_q show good agreements with the optimal iteration numbers $n_{\text{opt},h}$ and $n_{\text{opt},q}$, except for $n_q = 32 < n_{\text{opt},q} = 50$ when $p = 1\%$. However, the error at $n = n_q = 32$ ($E_2[q] = 0.0439$) is very close to the error at $n = 50$ ($E_2[q] = 0.0426$) and thus, for $p = 1\%$, it is reasonable to stop the iterations at $n = n_q = 32$ without much loss of accuracy. Moreover, as shown in Figures 6(c) and 6(d), $E_1[h^n]$ increases faster than $E_2[q^n]$ with increasing n, indicating that the recovery of $h(t)$ is less accurate and stable than the recovery of $q(t)$.

Figure 7 shows the estimated solutions of $h(t)$ and $q(t)$. In the case of no noise ($p = 0$), the results are presented after 50 iterations, whilst in the case of noisy data the results are presented after n_h and n_q iterations for $h(t)$ and $q(t)$, respectively. In the case of no noise, the numerical solutions agree well with the exact solutions (74) and
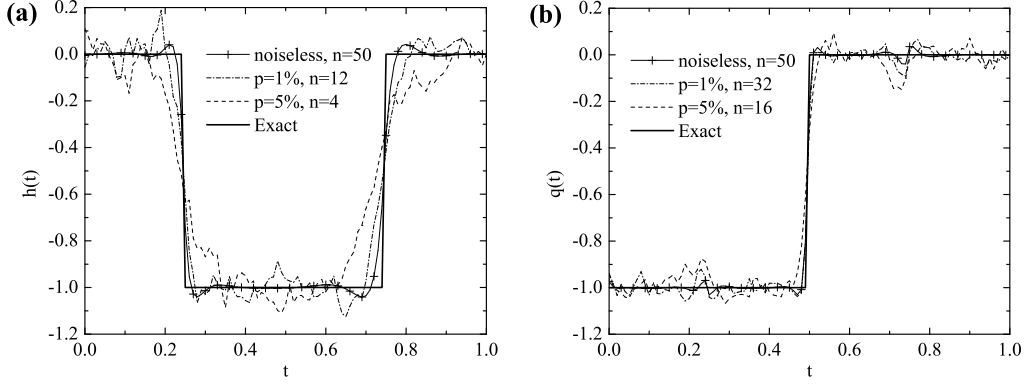
Figure 7. The inverse solutions of (a) the reaction coefficient $h(t)$ and (b) the heat flux $q(t)$, for $p \in \{0, 1\%, 5\%\}$ noise, for example 2.

(75). For noisy data, $p \in \{1, 5\}\%$, there are some deviations in the retrieved solutions especially at the discontinuity points, $t = 0.25$ and 0.75. By comparing the results of Figures 7(a) and 7(b), as anticipated before, it can be seen that the reconstruction of the heat flux $q(t)$ is more stable than that of the reaction coefficient $h(t)$ in the presence of the same noise level, and they both become more accurate as p decreases. The expected inaccuracy in $q(t)$ near the final time $t = T = 1$, [19], is not observed in Figure 7(b), because $x_2 = 0.1$ is quite close to the boundary $x = 0$ where the unknown heat flux is sought and also the initial guess $q^0(t)$ is zero. Nevertheless, inaccuracies near $t = T$ in the retrieved heat flux (2) will start to appear as the location x_2 of the thermocouple moves away from the boundary end $x = 0$.

7. Conclusions

In this paper, both the IHSP and the IHCP are solved to determine the unknown time-dependent reaction coefficient $h(t)$ of a nonlinear heat source and the heat flux $q(t)$, respectively, from two internal temperature measurements. Local existence and uniqueness of a classical solution to the IHSP are proved under the assumptions $(\mathbf{A}_1)$-$(\mathbf{A}_3)$ or $(\mathbf{A}'_1)$-$(\mathbf{A}'_3)$, which include that the derivatives of $g(u)$ up to the third order are Lipschitz continuous functions. The inverse solutions to the IHSP and the IHCP have been obtained via the CGM. For noisy data, regularization is achieved by stopping the iterations at a threshold dictated by the discrepancy principle. The stopping iteration numbers for estimating $h(t)$ are smaller than those for estimating $q(t)$. In addition, the sensitivity of the retrieved $h(t)$ to measurement noise is higher than that of $q(t)$. From the numerical results, it can be seen that the solutions of $h(t)$ and $q(t)$ to the corresponding inverse problems investigated are obtained efficiently and stably.

The more general case of recovering the space- and time-dependent reaction coefficient $h(x, t)$ from temperature measurements at many space locations is currently under investigation.

References

[1] O.M. Alifanov, *Solution of an inverse problem of heat conduction by iteration methods*, J. Eng. Phys. 26 (1974), pp. 471–476.

[2] O.M. Alifanov, *Inverse Heat Transfer Problems*, Science & Business Media, Berlin, 2012.

[3] J.V. Beck, B. Blackwell, and C.R. St. Clair, *Inverse Heat Conduction*, Wiley, New York, 1985.

[4] Y.Y. Belov, *Inverse Problems for Partial Differential Equations*, VSP, Utrecht, 2002.

[5] H.R. Busby and D.M. Trujillo, *Numerical solution to a two-dimensional inverse heat conduction problem*, Int. J. Numer. Methods Eng. 21 (1985), pp. 349–359.

[6] J.R. Cannon, *Structural identification of an unknown source term in a heat equation*, Inverse Problems 14 (1998), pp. 535–551.

[7] K. Cao and D. Lesnic, *Reconstruction of the perfusion coefficient from temperature measurements using the conjugate gradient method*, Int. J. Comput. Math. 95 (2018), pp. 797–814.

[8] G. Chi and G. Li, *Numerical inversions for a nonlinear source term in the heat equation by optimal perturbation algorithm*, Appl. Math. Comput. 216 (2010), pp. 2408–2416.

[9] R. Das, S.C. Mishra, T.B.P. Kumar, and R. Uppaluri, *An inverse analysis for parameter estimation applied to a non-Fourier conduction–radiation problem*, Heat Transf. Eng. 32 (2011), pp. 455–466.

[10] R. Das and K.T. Ooi, *Application of simulated annealing in a rectangular fin with variable heat transfer coefficient*, Inverse Probl. Sci. Eng. 21 (2013), pp. 1352–1367.

[11] R. Das, K. Singh, B. Akay, and T.K. Gogoi, *Application of artificial bee colony algorithm for maximizing heat transfer in a perforated fin*, Proc. Inst. Mech. Eng. E 232 (2016), pp. 38–48.

[12] M. Dehghan, *Finding a control parameter in one-dimensional parabolic equations*, Appl. Math. Comput. 135 (2003), pp. 491–503.

[13] Z.C. Deng, L. Yang, J.N. Yu, and G.W. Luo, *An inverse problem of identifying the coefficient in a nonlinear parabolic equation*, Nonlinear Anal. 71 (2009), pp. 6212–6221.

[14] A. Erdem, D. Lesnic, and A. Hasanov, *Identification of a spacewise dependent heat source*, Appl. Math. Model. 37 (2013), pp. 10231–10244.

[15] Z.C. Feng, J.K. Chen, Y. Zhang, and J.L. Griggs, *Estimation of front surface temperature and heat flux of a locally heated plate from distributed sensor data on the back surface*, Int. J. Heat Mass Transf. 54 (2011), pp. 3431–3439.

[16] A.P. Fernandes, M.B. dos Santos, and G. Guimarães, *An analytical transfer function method to solve inverse heat conduction problems*, Appl. Math. Model. 39 (2015), pp. 6897–6914.

[17] T.K. Gogoi and R. Das, *Inverse analysis of an internal reforming solid oxide fuel cell system using simplex search method*, Appl. Math. Model. 37 (2013), pp. 6994–7015.

[18] P.C. Hansen, *The truncated SVD as a method for regularization*, BIT Numer. Math. 27 (1987), pp. 534–553.

[19] D.N. Hào, *Methods for Inverse Heat Conduction Problems*, Peter Lang, Frankfurt am Main, 1998.

[20] A. Hasanov, *Identification of spacewise and time dependent source terms in 1D heat conduction equation from temperature measurement at a final time*, Int. J. Heat Mass Transf. 55 (2012), pp. 2069–2080.

[21] A. Hazanee, M.I. Ismailov, D. Lesnic, and N.B. Kerimov, *An inverse time-dependent source problem for the heat equation*, Appl. Numer. Math. 69 (2013), pp. 13–33.

[22] C.H. Huang, P.Y. Wu, and S. Kim, *A nonlinear inverse problem in estimating the poly-*

merization heat source of bone cements by an iterative regularization method, Inverse Problems 26 (2010), p. 065009.

[23] K.I. Khudaverdiyev and A.G. Alieva, *On the global existence of solution to one-dimensional fourth order nonlinear Sobolev type equations*, Appl. Math. Comput. 217 (2010), pp. 347–354.

[24] S.Y. Lee and T.W. Huang, *A method for inverse analysis of laser surface heating with experimental data*, Int. J. Heat Mass Transf. 72 (2014), pp. 299–307.

[25] D. Lesnic, *Identification of the time-dependent perfusion coefficient in the bio-heat conduction equation*, J. Inverse Ill-Posed Probl. 17 (2009), pp. 753–764.

[26] D. Lesnic and M. Ivanchov, *Determination of the time-dependent perfusion coefficient in the bio-heat equation*, Appl. Math. Lett. 39 (2015), pp. 96–100.

[27] C.N. Lin and J.Y. Jang, *A two-dimensional fin efficiency analysis of combined heat and mass transfer in elliptic fins*, Int. J. Heat Mass Transf. 45 (2002), pp. 3839 – 3847.

[28] L. Marin, L. Elliott, P.J. Heggs, D.B. Ingham, D. Lesnic, and X. Wen, *Analysis of polygonal fins using the boundary element method*, Appl. Thermal Eng. 24 (2004), pp. 1321–1339.

[29] M. Mohammadi, M.R. Hematiyan, and L. Marin, *Boundary element analysis of nonlinear transient heat conduction problems involving non-homogenous and nonlinear heat sources using time-dependent fundamental solutions*, Eng. Anal. Bound. Elem. 34 (2010), pp. 655–665.

[30] M.N. Ozisik and H.R.B. Orlande, *Inverse Heat Transfer: Fundamentals and Applications*, Taylor & Francis, New York, 2000.

[31] P.W. Partridge and L.C. Wrobel, *The dual reciprocity boundary element method for spontaneous ignition*, Int. J. Numer. Methods Eng. 30 (1990), pp. 953–963.

[32] S.V. Patankar, *Numerical Heat Transfer and Fluid Flow*, McGraw-Hill, New York, 1980.

[33] R.L. Potts, *Application of integral methods to ablation charring erosion - a review*, J. Spacecr. Rockets 32 (1995), pp. 200–209.

[34] R. Riganti and E. Savateev, *Solution of an inverse problem for the nonlinear heat equation*, Comm. Partial Differential Equations 19 (1994), pp. 1611–1628.

[35] E.G. Savateev and R. Riganti, *Inverse problem for the nonlinear heat equation with the final overdetermination*, Math. Comput. Model. 22 (1995), pp. 29–43.

[36] E.P. Scott, P.S. Robinson, and T.E. Diller, *Development of methodologies for the estimation of blood perfusion using a minimally invasive thermal probe*, Meas. Sci. Technol. 9 (1998), pp. 888–897.

[37] A. Shidfar, B. Jazbi, and M. Alinejadmofrad, *Numerical approximation of a non-linear source term for an inverse parabolic problem*, Comput. Appl. Math. 34 (2015), pp. 363–373.

[38] A. Shidfar, G.R. Karamali, and J. Damirchi, *An inverse heat conduction problem with a nonlinear source term*, Nonlinear Anal. 65 (2006), pp. 615–621.

[39] E.A. Sudicky, *The Laplace transform Galerkin technique: A time-continuous finite element theory and application to mass transport in groundwater*, Water Resour. Res. 25 (1989), pp. 1833–1846.

[40] A.N. Tikhonov and V.Y. Arsenin, *Solutions of Ill-Posed Problems*, Winston, Washington, D. C., 1977.

[41] D. Trucu, D.B. Ingham, and D. Lesnic, *Inverse time-dependent perfusion coefficient identification*, J. Phys. Conf. Ser. 124 (2008), p. 012050.

[42] D. Trucu, D.B. Ingham, and D. Lesnic, *Space-dependent perfusion coefficient identification in the transient bio-heat equation*, J. Eng. Math. 67 (2010), pp. 307–315.

[43] N.H. Tuan, V.V. Au, D. Lesnic, and T.Q. Viet, *Regularization of nonlinear sideways heat equation*, submitted to IMA J. Appl. Math. .

[44] S. Wang and Y. Lin, *A finite difference solution to an inverse problem for determining a control function in a parabolic partial differential equation*, Inverse Problems 5 (1989), pp. 631–640.

[45] S. Zhu and P. Satravaha, *An efficient computational method for modelling transient heat conduction with nonlinear source terms*, Appl. Math. Model. 20 (1996), pp. 513–522.

[46] S. Zhu, Y. Zhang, and T.R. Marchant, *A DRBEM model for microwave heating problems*, Appl. Math. Model. 19 (1995), pp. 287–297.

[47] Y. Zhu, F. Yi, S. Meng, L. Zhuo, W. Pan, and J. Zhang, *Multiphysical behavior of a lightweight ablator: Experiments, modeling, and analysis*, J. Spacecr. Rockets 544 (2017), pp. 1–10.

[48] L. Zhuo, F. Yi, and S. Meng, *An inverse method for the estimation of a long-duration surface heat flux on a finite solid*, Int. J. Heat Mass Transf. 106 (2017), pp. 1087–1096.